Canadian Conference - Pacific Conference on Earthquake Engineering 2023

Vancouver, British Columbia

June 25th – June 30th, 2023

Metro Vancouver Liquefaction Hazard Mapping

Alireza Javanbakht[1*], Jamal Assaf[2], Mohammad Salsabili[3], Abouzar Sadrekarimi[4], Hadi Ghofrani[5], Sheri Molnar[6]

[1]PhD Student, Department of Earth Sciences, University of Western Ontario, London, Ontario, Canada
[2]Geotechnical Engineer, Golder/WSP, Vancouver, British Columbia, Canada
[3]Research Scientist, Department of Earth Sciences, University of Western Ontario, London, Ontario, Canada
[4]Associate Professor, Department of Civil and Environmental Engineering, University of Western Ontario, London, Ontario, Canada
[5]Adjunct Research Professor, Department of Earth Sciences, University of Western Ontario, London, Ontario, Canada
[6]Associate Professor, Department of Earth Sciences, University of Western Ontario, London, Ontario, Canada
[*]ajavanba@uwo.ca and smolnar8@uwo.ca (Corresponding Authors)

ABSTRACT

To evaluate regional seismic-induced liquefaction hazard in a probabilistic framework, it is necessary to consider all earthquake scenarios to define the probability of liquefaction for a specific return period. We use approximately 809 cone penetration tests (CPTs) and 92 shear-wave velocity profiles (V_s) across the study area in Metro Vancouver to calculate the liquefaction potential index (LPI) which has two thresholds (> 5 as occurrence of sand boils, and > 15 as occurrence of severe liquefaction). The latest CPT-based simplified procedure and Vs-based liquefaction triggering method are applied in this study. The LPI is calculated from the depth-weighted factor of safety over the upper 20 m of the ground. We perform probabilistic seismic hazard analyses (PSHA) using the 6th national seismic hazard model (adopted in the 2020 National Building Code) for 16 locations at two selected Vs_{30} values (170, 250 m/s) to obtain the maximum ground acceleration (a_{max}) and the associated magnitude (M) of each earthquake scenario for two selected return periods. We then perform our probabilistic liquefaction hazard analyses (PLHA) for the 900 *in situ* CPT and V_s locations to obtain the annual probability of liquefaction occurrence at the two selected return periods. The incremental mean annual rate of exceedance for a_{max} from PSHA results and the probability of the LPI greater than a threshold value conditioned on a_{max} and M produces the probabilistic liquefaction hazard curves for each CPT and V_s site. Spatial variance in the probabilistic LPI is mapped via interpolation within similar geologic units to achieve regional liquefaction hazard mapping. Probabilistic liquefaction hazard maps are produced for 2% and 10% probabilities of exceedance in 50 years hazard levels for Metro Vancouver. The seismic-induced liquefaction potential is the highest for Fraser River sediments in Richmond, Delta, and along the Fraser River channels, and severe liquefaction (e.g., lateral spreading) could occur in sloping areas. The liquefaction potential elsewhere throughout Metro Vancouver is lower due to soil conditions with lower liquefaction susceptibility and deeper groundwater levels.

Keywords: Liquefaction, Greater Vancouver, Probabilistic liquefaction hazard, Liquefaction simplified procedure, Probabilistic seismic hazard analyses keywords separated by commas.

INTRODUCTION

Metro Vancouver lies in one of the most seismically active regions in Canada. The existence of loose sand and silty layers and shallow groundwater table in most parts of the study area could lead to liquefaction initiation. Therefore, the evaluation of liquefaction in the study area is necessary. Liquefaction hazard mapping of prone regions is increasingly being incorporated into earthquake hazard mitigation practice. To prepare the liquefaction hazard map, we need a parameter predicting the hazard classification. Iwasaki et al. [1] introduced the liquefaction potential index (LPI) that determines the liquefaction potential along a soil profile from the ground surface to a depth of 20 m. The surface damages from liquefaction at depths greater than 20 m are rarely observed/reported. LPI is proportional to the amount by which the factor of safety against liquefaction is less than one, and the thickness and proximity of liquefied layers to the surface. Toprak and Holzer [2], Sonmez [3], Hiedari and Andrus [4], Rahman et al. [5] and Papathanassiou et al. [6] have applied LPI to classify the liquefaction potential hazards and generate

liquefaction hazard maps. Geotechnical *in-situ* tests such as cone penetration testing (CPT), standard penetration test (SPT), and shear wave velocity (V_s) profiles are typically used to obtain the factor of safety against liquefaction for each layer and then the LPI value for the whole soil profile. The CPT has the big advantage of tracking thin sand layers compared to SPT and Vs data.

Simplified methods provide the evaluation of liquefaction triggering potential. In this procedure, the cyclic stress ratio (CSR) proposed by Seed and Idriss [7] represents the seismic loading from earthquake-induced liquefaction, while the cyclic resistance ratio (CRR) shows the soil capacity during soil shaking. If the CSR is greater than CRR, then the soil layer will liquefy. When using the simplified method, the big question becomes which earthquake magnitude (M_w), and maximum ground acceleration (a_{max}) should be applied for liquefaction assessment. The conventional approach suggests using the deaggregation results from the probabilistic seismic hazard (PSHA) for a_{max} at the return period of interest and considering mean or modal M_w (Franke et al. [8]). In this way, the ground motions are determined probabilistically, and the liquefaction evaluation is performed deterministically. In addition, the single selection for a combination of a_{max} and M_w results in inconsistent predicted hazards across different seismic environments (Juang et al. [9]; Kramer and Mayfield [10]; Franke and Wright [11]). It means overestimation of liquefaction hazard in low active seismic areas. To overcome these issues, Kramer and Mayfield [12] introduced a performance-based procedure for evaluating liquefaction potential based on the Performance-Based Earthquake Engineering (PBEE) design. Their approach integrates the factor of safety against liquefaction based on a seismic hazard curve and forms the liquefaction hazard curve from the annual rate of liquefaction. All possible ground motions are considered in the liquefaction assessment rather than a single shaking level with one a_{max} and one M_w. The corresponding mean annual rate (or inverse of the return period) of interest can be obtained for design purposes. Kramer and Mayfield [10] incorporated an SPT-based methodology by Cetin et al. [13] into the PBEE framework and constructed a probability of non-exceedance of a factor of safety against liquefaction. They compared the likelihood of liquefaction triggering for some cities in the USA with different seismicity. Franke and Wright [11] developed an alternative relationship for generating an FSL curve using the Boulanger and Idriss [14] probabilistic liquefaction triggering model. Cramer et al. [15] incorporated the LPI into the PSHA formula and generated the liquefaction hazard map of Memphis, USA considering the probability of LPI exceeding 5 and 15 within each geology unit. Goda et al. [16] demonstrated the methodology for representing the probability of LPI exceeding a threshold value considering joint probability distribution of a_{max} and M_w for four Canadian cities and obtained the return period of sand boiling (LPI=5) and lateral spreading (LPI=15) from calculated liquefaction hazard curves. Green et al. [17] incorporated the modified version of LPI into the PBEE approach and derived the liquefaction hazard for two specific return periods for the Groningen region in the Netherlands. Geyin et al. [18] followed the same approach to compute the annual probability of LPI using a CPT site in Seattle and the LPI was calculated from CPT-based methodology by Boulanger and Idriss [19].

In this study, we generate probabilistic liquefaction hazard maps for Metro Vancouver, British Columbia, Canada for 2% and 10% probabilities of exceedance in 50 years based on the 6th national seismic hazard model (2020 National Building Code of Canada). These probabilistic liquefaction hazard maps are part of the Metro Vancouver seismic microzonation mapping project (https://metrovanmicromap.ca, Molnar et al. [20]). The latest CPT- and Vs-based liquefaction triggering models are used to obtain the factor of safety for each layer and then the LPI values for a whole 20 m of the soil profile. We use the direct interpolation technique to obtain the LPI values for neighborhood points for regions with sufficient in-situ measurements.

SURFICIAL GEOLOGY OF METRO VANCOUVER AND DATA

The regional geology of Metro Vancouver consists of Tertiary and older bedrock with variable Quaternary sediments including Pleistocene and older inter/glacial sediments and Holocene sediments. The Fraser Lowland is predominantly the result of depositional processes that occurred following the last deglaciation 11,000 to 13,500 years ago, and to a lesser extent during the Holocene Epoch. Quaternary sediments cover the irregular, glacially scoured Tertiary sediment bedrock of the Georgia Basin that dips southward beneath Greater Vancouver from their exposure along the North Shore in contact with the Pre-Tertiary Coast Mountains plutonic igneous rocks (Molnar [21]). During the Quaternary Period, three major glaciations occurred with interglacial cycles, with the Fraser glaciation (~13,000 years ago) being the last major glaciation in British Columbia. Each major glaciation was accompanied by isostatic changes caused by glacier formation and decay. Low-lying land regions such as the Fraser Lowlands were repeatedly transgressed and regressed by the sea over the Pleistocene Epoch, and marine, glaciomarine, and deltaic sediments were deposited in complex associations with glacial, glaciofluvial, and ice-contact elements. The changing climate caused the deposition of a body of sandy outwash known as Quadra Sand, which can be up to 100 meters deep, in the Strait of Georgia at the start of the Fraser Glaciation (Armstrong and Clague [22]; Clague [23]). This deposit is made up of well-sorted fine to medium cross-stratified sand with minor interbedded layers of silt and gravel in the lower and upper parts, respectively. Quadra Sand was deposited progressively from northwest to southeast down the Strait of Georgia, according to paleocurrent data, sand mineralogy, and radiocarbon dates, resulting in a decrease in age from northwest to southeast (Clague [23]). These deposits can be seen in Coquitlam, Vancouver, West Vancouver, and North Vancouver. Hicock and Armstrong (1981) indicate that tills and related glacial sediments were deposited during two separate glaciations, the Coquitlam Drift and the Vashon Drift. Coquitlam Drift was formed by glaciers advancing out of the Coast Mountains and

across Fraser Lowland during the early phase of the Fraser Glaciation. Vashon Drift was formed when glaciers reached their late Wisconsin climax positions, and it is overlain by Coquitlam Drift. Deglaciation began around 13,000 years ago and the Fraser Lowland completed its deglaciation about 11,000 years ago (Clague et al. [24]). During deglaciation, three lithostratigraphic units were deposited in Fraser Lowland: The Fort Langley Formation, Capilano Sediments, and Sumas Drift. The Fort Langley Formation is a thick (100+ m) succession of interbedded glaciomarine, deltaic, littoral, glacial, and ice-contact deposits that were produced in close conjunction with an ice front that fluctuated in the central and eastern Fraser Lowlands for over 2000 years. The Capilano Sediments, which exist in the western Fraser Lowland, are thin beneath Upland areas and lack till, ice-contact sediments, and subaqueous outwash indicating they are deposited in distal environments. The primary sediment type of the Capilano Sediments, which were created by meltwater streams originating in the Coast Mountains, is clayey and sandy silt with scattered granitic rock pebbles and cobbles, whereas deltaic and outwash deposits of the Fort Langley Formation and Sumas Drift were formed by meltwater from decaying glaciers in the central and eastern Fraser Lowland and thereby contain an abundance of Cascades Mountains rocks sometimes as drop stones. As the sea continued to retreat relative to the land, large settling basins of deserted glacial ice formed. Since the lowland was filled with fluvial and deltaic materials, a floodplain extended westward along the Fraser River valley to around the Fraser River's current elevation. After the last glaciation, the Fraser River began to form its delta into the Salish Sea about 10 thousand years ago (Clague et al. [24]). The Fraser River delta was formed entirely during the Holocene Epoch (Clague et al. [25]).

We compiled 808 CPT and 92 Vs profiles from our geodatabase (Molnar et al. [20]) and Figure 1 shows the location of these sites on a simplified quaternary geology map of Metro Vancouver. In Richmond and Delta cities, there is a good density of available in-situ measurements, while in other areas we have fewer data. Of the 900 CPT and Vs soundings, 728 of them have a depth greater than 20 m. Of the soundings that do not reach 20 m, 65 profiles terminate at 15-20 m and 75 CPTs reach depths of 10-15 m. We also used 32 CPT and V_s profiles with a depth of less than 10 m, particularly in areas with a lower amount of data. The nearby boreholes, if available, provide fines content, grain size distribution, water content, and plasticity. The groundwater table (GWT) for liquefaction assessment is inferred from *in situ* tests if reported, otherwise, it would be obtained from a regionally interpolated map of the groundwater table for the Greater Vancouver area. Soil above the groundwater table would not liquefy. In most areas in Richmond and Delta, GWT is less than 3 m and in some sites, it has a depth of less than a meter. GWT changes from less than 3 m to 10 m in Vancouver and Burnaby.

METHODOLOGY

In this section, we go through the CPT- and Vs-based methodology and provide some details for each of them. We then show how to calculate LPI values for each site. Finally, we present the probabilistic method for achieving the annual rate of exceedance of LPI in the PBEE framework. The implemented methodology underwent professional peer review with the Engineers and Geoscientists of British Columbia, EGBC (Molnar et al. [26]).

The I_c value proposed by Robertson and Cabal [27] distinguishes liquefiable and no-liquefiable layers for CPT sites. I_c is calculated via normalized cone resistance and sleeve friction ratios considering the stress exponent ^{n} which changes from 0.5 in sands to 1.0 in clays. In this study, if I_c is greater than 2.60, then the soil is too clayey to liquefy. However, Youd et al. [28] suggest that soil layers with $I_c > 2.4$ should be sampled and tested to investigate the soil behavior type. Therefore, it is suggested that every CPT sounding should be accompanied by one borehole with soil samples to perform laboratory tests for defining FC. We obtained FC from adjacent boreholes and if FC data are not provided in geotechnical reports, then the relationship by Boulanger and Idriss [19] is used to estimate FC. However, experiences show that defining fines content (FC) from correlation with I_c is problematic.

CPT-based Liquefaction Triggering Model

We apply the CPT-based methodology by Boulanger and Idriss [19] to calculate FS against liquefaction for each soil layer from CPT profiles. The measured cone resistance is corrected for pore water pressure acting on the cone (u_2) to obtain corrected cone resistance, q_t. For sandy soils, the magnitude of this correction is small, while in soft clay layer is significantly large. In our analyses, pore water correction is applied whenever the value of u_2 is measured, and we use the term q_c with the understanding that the correction has been performed. The q_c term is corrected for overburden stress by applying the C_N overburden correction factor of Boulanger [29] which requires an iterative procedure. The normalized tip resistance for silty sands should be corrected to an equivalent clean sand term (q_{c1Ncs}). The equivalent clean sand adjustment, Δq_{c1N} is considered in this simplified method for the effect of fines content (FC) on cyclic stress ratio and cone penetration resistance from Boulanger and Idriss [19]. Δq_{c1N} and q_{c1Ncs} are estimated from Eqs. 1a and 1b:

$$\Delta \mathbf{q_{c1N}} = \left(\mathbf{11.9} + \frac{\mathbf{q_{c1N}}}{\mathbf{14.6}}\right) \exp\left(\mathbf{1.63} - \frac{\mathbf{9.7}}{\mathbf{FC+2}} - \left(\frac{\mathbf{15.7}}{\mathbf{FC+2}}\right)^{\mathbf{2}}\right) \tag{1a}$$

$$\mathbf{q_{c1Ncs}} = \mathbf{q_{c1N}} + \Delta \mathbf{q_{c1N}} \tag{1b}$$

The CRR is computed from the latest methodology by Boulanger and Idriss (2014) with Eq. (2):

$$\mathbf{CRR_{M=7.5,\sigma'_v=1atm}} = \mathbf{exp}\left(\frac{q_{c1Ncs}}{113} + \left(\frac{q_{c1Ncs}}{1000}\right)^2 - \left(\frac{q_{c1Ncs}}{140}\right)^3 + \left(\frac{q_{c1Ncs}}{137}\right)^4 - \mathbf{2.80}\right) \quad (2)$$

Seed and Idriss [7] proposed the seismic demand loading in the simplified procedure and CSR for a reference condition of Mw=7.5 and $\sigma'_v = 1atm$ is calculated from Eq. (3):

$$\mathbf{CSR_{M=7.5,\sigma'_v=1atm}} = \mathbf{0.65}\left(\frac{a_{max}}{g}\right)\left(\frac{\sigma_{v0}}{\sigma'_{v0}}\right)\frac{r_d}{MSF.k_\sigma} \quad (3)$$

where a_{max} is the maximum acceleration applied by the earthquake, g is the acceleration of gravity, r_d is the stress reduction factor, σ_{v0}, and σ'_{v0} are total and effective vertical stresses, respectively, at the depth of interest, k_σ is an effective overburden stress correction factor, and MSF is magnitude scale factor by Boulanger and Idriss [19].

The stress reduction factor, r_d, was obtained from the relationship by Idriss [30]. The revised MSF extends to magnitude 9 and could consider the Cascadia subduction zone event in the simplified estimation of FS. The Boulanger and Idriss [19] MSF will produce higher CSR for small earthquake magnitudes and is obtained from Eq. (4):

$$\mathbf{MSF} = \mathbf{1} + (\mathbf{MSF_{max}} - \mathbf{1})[\mathbf{8.64}\,\mathbf{exp}\left(\frac{-M_w}{4}\right) - \mathbf{1.325}] \quad (4a)$$

$$\mathbf{MSF_{max}} = \mathbf{1.09} + \left(\frac{q_{c1Ncs}}{180}\right)^3 \leq \mathbf{2.2} \quad (4b)$$

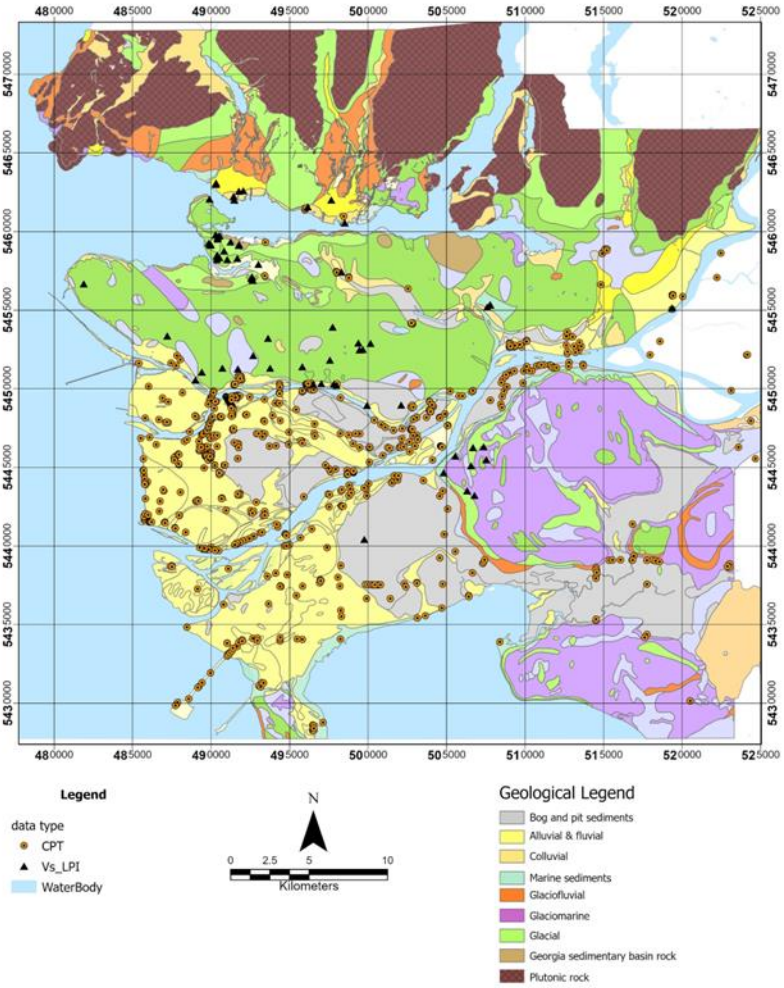

Figure 1- The Quaternary geological map of Metro Vancouver with CPT and Vs locations

Vs-based Liquefaction Triggering Model

For in situ V_s, we apply the V_s-based liquefaction triggering model by Andrus et al. [31] to obtain the FS. We should note that the V_s method for liquefaction assessment is the least sensitive method, and it has issues in differentiating the effects of FC.

The CSR at a particular depth in a soil deposit is calculated from Eq. (3). Here the MSF by Youd et al. [28] is used from Eq. (5):

$$\mathbf{MSF} = (\frac{\mathbf{M_w}}{\mathbf{7.5}})^{\mathbf{-2.56}} \tag{5}$$

This MSF is applicable for M_w=5.5 and M_w=8-8.5. We consider the M_w in our study from M_w=4.9 to M_w=9.0 which is wider than the range recommended by Youd et al. [28]. V_s values are corrected by applying an overburden stress factor (Roberston et al. [32]):

$$\mathbf{V_{S1}} = \mathbf{V_S C_{VS}} = \mathbf{V_s}(\frac{\mathbf{P_a}}{\boldsymbol{\sigma}_\mathbf{v}^{\prime}})^{\mathbf{0.25}} \tag{6}$$

where V_{s1} is stress-corrected shear-wave velocity, C_{vs} is an overburden pressure correction factor and P_a is reference stress of 100 kPa. The maximum C_{vs} factor is 1.4 which is applied to shallow depths.

The maximum upper value of V_{s1} for liquefaction evaluation presents a limit that liquefaction would not occur above it in a V_s liquefaction initiation model (V_{s1}^*). This assumption is equivalent to the assumption the liquefaction would not be possible for a soil layer with an SPT number above 30 (Youd et al. [33]). Andrus et al. [31] suggested the following correlations for estimating the V_{s1}^* considering the FC range:

$$\mathbf{V_{S1}^*} = \mathbf{215\ m/s} \qquad \mathbf{FC} \leq \mathbf{5}\% \tag{7a}$$

$$\mathbf{V_{S1}^*} = \mathbf{215 - 0.5(FC - 5)}\ \frac{\mathbf{m}}{\mathbf{s}} \qquad \mathbf{5}\% < \mathbf{FC} < \mathbf{35}\% \tag{7b}$$

$$\mathbf{V_{S1}^*} = \mathbf{200\ m/s} \qquad \mathbf{FC} \geq \mathbf{35}\% \tag{7c}$$

In the last step, we determine the CRR in V_s-based methodology from Eq. (8):

$$\mathbf{CRR} = \mathbf{MSF}\left\{\mathbf{0.022}(\frac{\mathbf{K_{a1}V_{S1}}}{\mathbf{100}})^{\mathbf{2}} + \mathbf{2.8}(\frac{\mathbf{1}}{\mathbf{V_{S1}^* - (K_{a1}V_{S1})}} - \frac{\mathbf{1}}{\mathbf{V_{S1}^*}})\right\}\mathbf{K_{a2}} \tag{8}$$

where K_{a1} and K_{a2} are age correction factors to extend the relationship for uncemented Holocene-age soil to older soils.

LPI Determination

LPI represents the cumulative liquefaction potential of the soil column from ground surface to 20 m depth and computed from Eq. (9):

$$\mathbf{LPI} = \int_0^{\mathbf{20}} \mathbf{F_L w(z) dz} \tag{9a}$$

$$\mathbf{F_L} = \mathbf{1 - FS} \qquad \mathbf{FS} \leq \mathbf{1} \tag{9b}$$

$$\mathbf{F_L} = \mathbf{0} \qquad \mathbf{FS} > \mathbf{1} \tag{9c}$$

where *z* is the depth from the ground surface in meters and the weighting factor, w(z), is a linear function of depth and it changes from 10 at the ground surface to 0 at a depth of 20 m.

LPI ranges from 0 to 100 and classifies the liquefaction hazard into very low (LPI = 0), low (0 < LPI ≤ 5), high (5 < LPI ≤ 15), and very high (LPI > 15) following Iwasaki et al. [1] suggestions.

PBEE Framework

As we mentioned earlier, instead of using a single combination of a_{max} and M_w in FS calculation, we consider all ground motion hazard levels affecting the study region. Three types of earthquakes affect the study area including shallow crustal earthquakes within the continental North American Plate (depth 20 km), deeper intraslab earthquakes within the subducting Juan de Fuca plate (depth 45 - 65 km), and interface earthquakes at the Cascadia subduction boundary with a maximum considered M_w of 9.2–9.3. We perform PSHA with OpenQuake engine considering the 6th national seismic hazard model (adopted in the 2020 National Building Code) for 16 locations at two selected V_{s30} values (170, 250 m/s) to obtain a_{max} and the associated M_w of each earthquake scenario. In the 2020 NBCC, probabilistic ground motions are computed directly from V_{s30} (time-averaged shear wave velocities of the upper 30 m) instead of using seismic site classes. Hence, we obtained V_{s30} for each CPT and Vs site from our geodatabase. We then incorporate LPI into the PSHA integral and obtain the annual probability of LPI:

$$\boldsymbol{\lambda}_{\mathbf{LPI}} = \sum_{\mathbf{j=1}}^{\mathbf{N_{Mw}}} \sum_{\mathbf{i=1}}^{\mathbf{N_{amax}}} \mathbf{P}\left(\mathbf{LPI} > \mathbf{lpi}\middle|\mathbf{a_{max_i}}, \mathbf{m_{w_j}}\right) \Delta\boldsymbol{\lambda}_{\mathbf{a_{max_i}, m_{w_j}}} \tag{10}$$

where N_{Mw} and N_{amax} are the numbers of magnitude and a_{max} increments into which the computed hazard space is subdivided, $P\left(LPI > lpi\middle|a_{max_i}, m_{w_j}\right)$ is the binomial probability that LPI exceeds some threshold value conditioned on a_{max} and M_w,

$\Delta\lambda_{a_{max_i},m_{w_j}}$ is the incremental mean annual rate of exceedance for intensity measure, a_{maxi} and m_{wj}. We derive the values of $\lambda_{a_{max_i},m_{w_j}}$ following the procedure by Kramer and Mayfield [10]. In this approach, the incremental rate of exceedance is distributed for magnitude according to the results of deaggregation analyses.

RESULTS

We followed the explained CPT- and V_s-based liquefaction triggering steps and performed the probabilistic liquefaction hazard analyses (PLHA) for a total number of 900 CPT and Vs sites to obtain the annual probability of liquefaction occurrence. From the constructed PLHA curve, we could select LPI values for the return periods of interest. In this study, we obtained the LPI values from the liquefaction hazard curve for the return periods of 476 and 2475 years. Figure 2 shows the PLHA curve for one site in Richmond city as an example. As can be seen, the LPI values corresponding to 10% and 2% POE are 22 and 35, respectively. These values of LPIs categorize the liquefaction hazard as very high for both selected return periods.

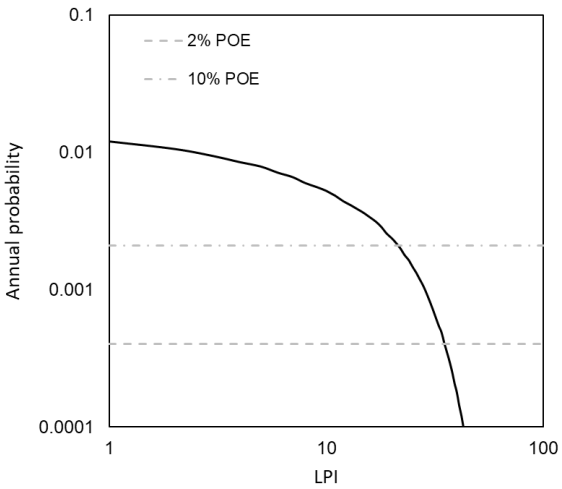

Figure 2- Liquefaction hazard curve for one CPT site in Richmond.

We obtained the liquefaction hazard curves for all sites and derived the LPI values for two selected return periods. Figures 3 and 4 show the locations of distributed LPIs for 2% and 10% POEs in 50 years, respectively. Most of the LPI values are > 15 in Richmond and Delta. In the east of Richmond, we have low LPI values due to thick non-liquefiable peat and silt cap layers even with very low cone resistance. In some parts of surrey and Vancouver, the LPI sites have zero values meaning non-liquefiable sites. North Vancouver region has sites ranging from very high to very low liquefaction hazards. The higher density of in-situ data in Richmond and Delta allows us to use the direct geostatistical interpolation technique to estimate the LPIs for areas without CPT and Vs data. This method disregards geological boundaries and works well with good spatial coverage and density of LPI values such as in Richmond but may not be applicable elsewhere in Metro Vancouver. Therefore, we obtained the average LPI for each geology unit and classified the liquefaction hazard based on the suggestions by Iwasaki et al. (1982).

Figures 5 and 6 show the liquefaction hazard mapping of the Metro Vancouver area for 2% and 10% POE in 50 years. As expected, most areas in Richmond and Delta have very high and high hazards of liquefaction. These high LPI values show a high risk of sand boil and lateral spreading. The young sand layers and thick layers of interbedded sand layers combined with a shallow water table result in a high potential for liquefaction in these areas. In Vancouver, most parts show very low LPI values and are grouped into very low and low hazards of liquefaction. The reason could be the older sediments and deeper groundwater table.

CONCLUSIONS

Instead of following the conventional liquefaction hazard evaluation and using a single combination of a_{max} and M_w, we applied the PBEE framework to obtain the liquefaction hazard curve for each CPT and V_s site. Thus, we considered the contribution of all earthquake hazards in our study. We presented probabilistic liquefaction hazard mapping of Metro Vancouver for 2% and 10% POEs in 50 years based on the 6th national seismic hazard model (2020 NBCC). These probabilistic liquefaction potential maps demonstrate that most of Richmond and Delta correspond to high to very high liquefaction triggering hazard and most of Vancouver and Surrey have very low liquefaction triggering hazard. These probabilistic seismic-induced liquefaction hazard maps are part of the Metro Vancouver seismic microzonation mapping project (Molnar et al. [20]).

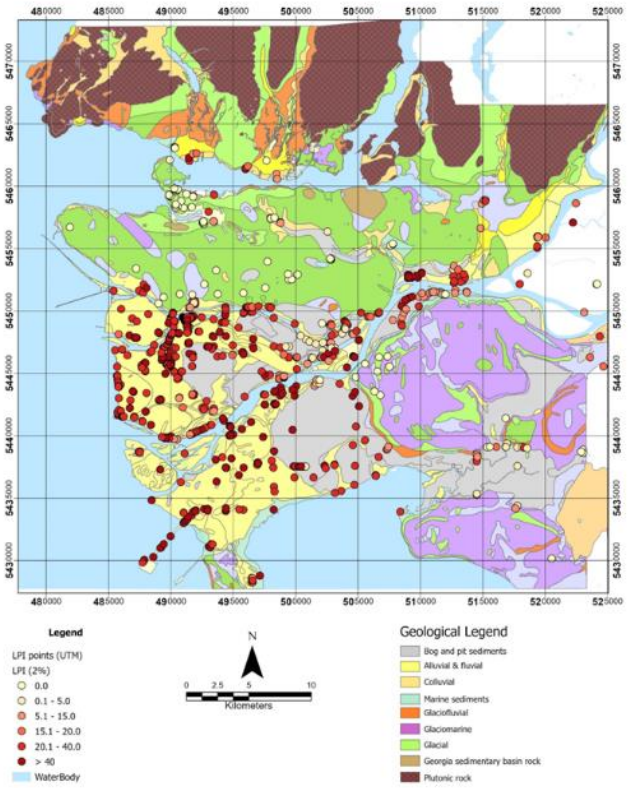

Figure 3- LPI values distributed across Metro Vancouver for 2% POE in 50 years.

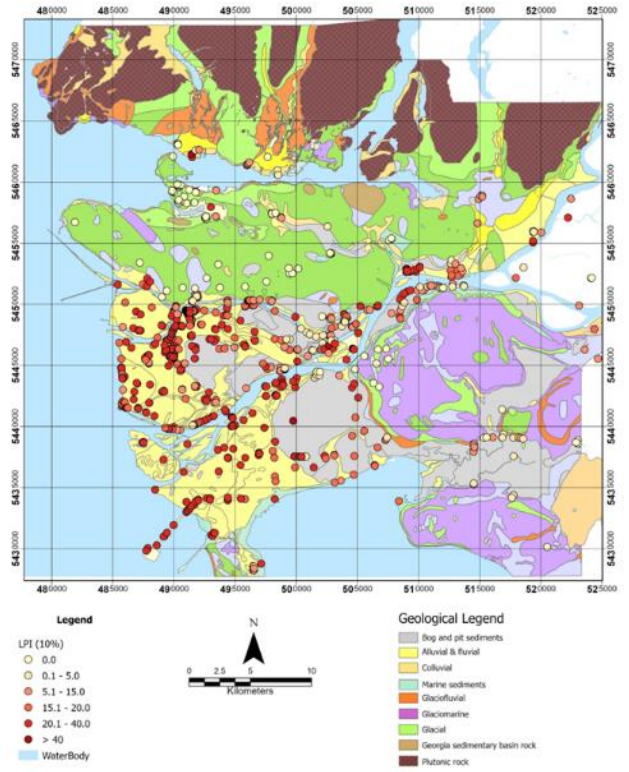

Figure 4- LPI values distributed across Metro Vancouver for 10% POE in 50 years.

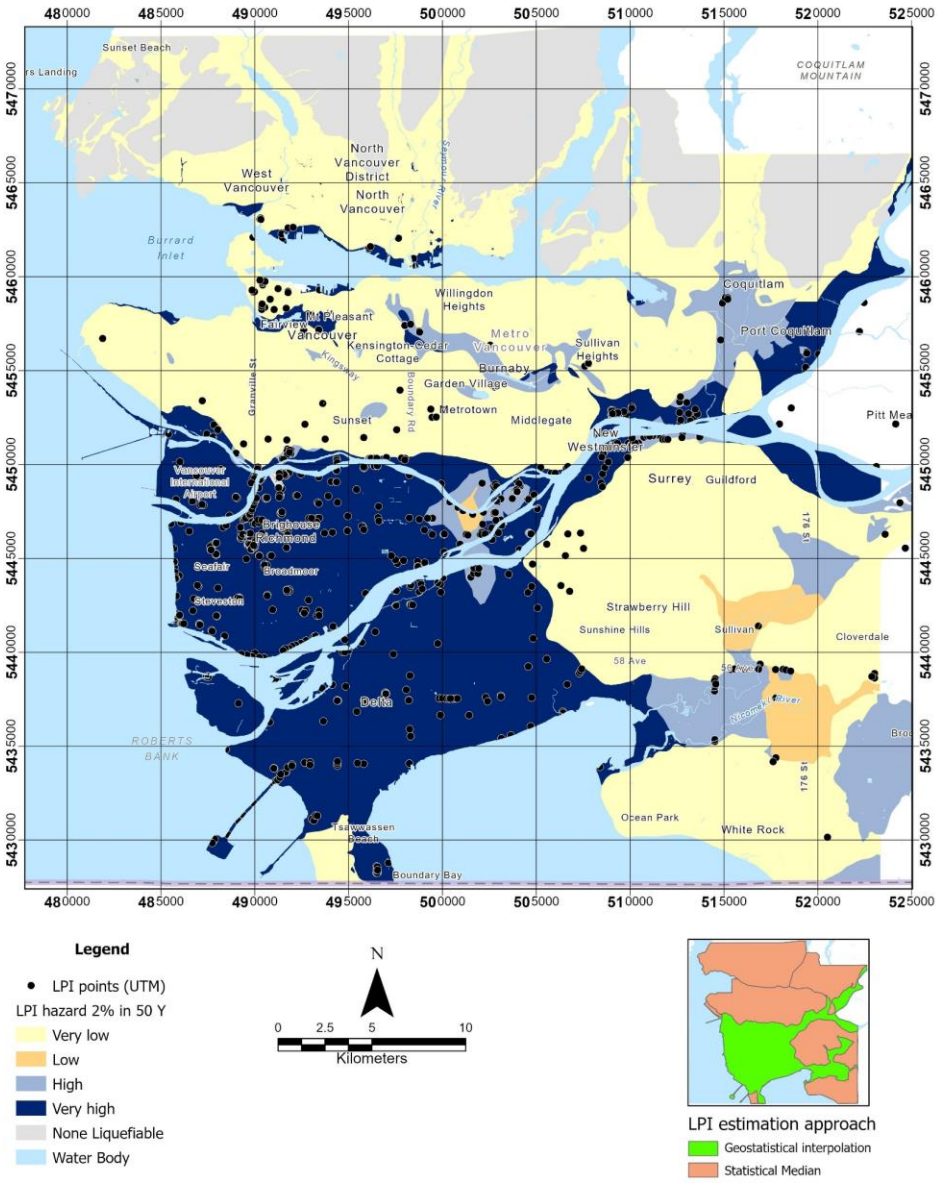

Figure 5- Probabilistic liquefaction hazard mapping of Metro Vancouver with LPI for 2% POE in 50 years.

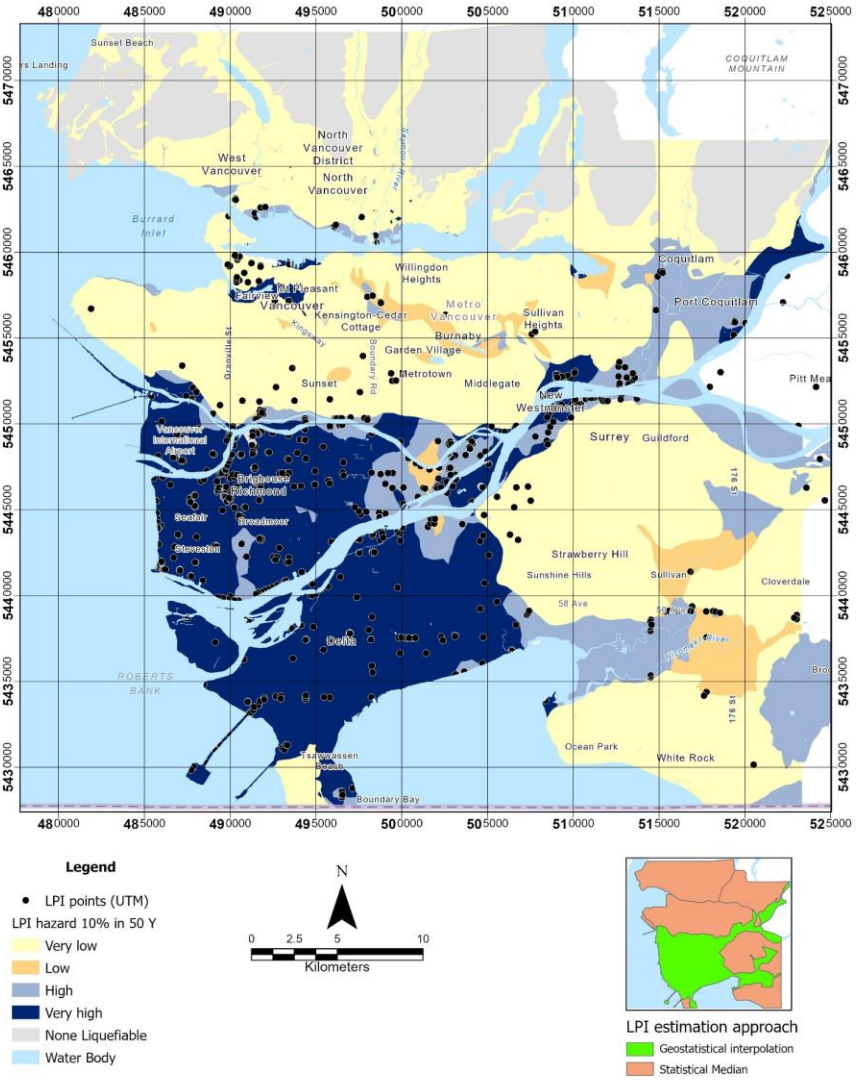

Figure 6- Probabilistic liquefaction hazard mapping of Metro Vancouver with LPI for 10% POE in 50 years.

ACKNOWLEDGMENTS

We gratefully acknowledge multiple agencies, organizations, municipalities, and individuals that provided both public and private sources of CPT data to the Metro Vancouver seismic microzontion project. Project funding was provided by the Institute for Catastrophic Loss Reduction (ICLR) with support from the BC Ministry of Emergency Management and Climate Readiness (EMCR).

REFERENCES

[1] Iwasaki T., Tokida, K., Tatsuoka, F., Watanabe, S., Yasuda, S. and Sato, H. 1982. "Microzonation for soil liquefaction potential using simplified methods". *In: Proceedings of the third international earthquake microzonation conference*, Seattle, WA, 3, 1319–30.

[2] Toprak, S. and Holzer T.L., 2003. "Liquefaction potential index: field assessment". *Journal of Geotechnical & Geoenvironmental Engineering*, 129 (4), 315–22.

[3] Sonmez, H. 2003. "Modification of the liquefaction potential index and liquefaction susceptibility mapping for a liquefaction-prone area (Inegol, Turkey)". *Environmental Geology*, 44 (7): 862–71.

[4] Heidari, T. and Andrus, R.D., 2010. "Mapping liquefaction potential of aged soil deposits in Mount Pleasant, South Carolina". *Engineering Geology*, 112 (1): 1-12.

[5] Rahman, M.Z., Siddiqua, S. and Kamal, ASMM., 2015. "Liquefaction hazard mapping by liquefaction potential index for Dhaka City, Bangladesh". *Engineering Geology*, 188, 137–147.
[6] Papathanassiou, G., Valkaniotis, S., Chaztipetros, A. and Pavlides, S., 2017. "Liquefaction susceptibility map of Greece". *Bulletin of the Geological Society of Greece*, 43 (3): 1383–1392.
[7] Seed H.B. and Idriss I.M., 1971. "Simplified procedure for evaluation soil liquefaction potential". *Journal of the Soil Mechanics and Foundations Division*, ASCE 97, 1249–1273 SM9.
[8] Franke, K.W., Ulmer, K.J., Ekstrom, L.T. and Meneses, J.F., 2016. "Clarifying the differences between traditional liquefaction hazard maps and probabilistic liquefaction reference parameter maps". *Soil Dynamics and Earthquake Engineering*, 90, pp.240-249.
[9] Juang, C.H., Li, D.K., Fang, S.Y., Liu, Z. and Khor, E.H., 2008. "Simplified procedure for developing joint distribution of a_{max} and M_w for probabilistic liquefaction hazard analysis". *Journal of Geotechnical and Geoenvironmental Engineering*, 134(8), pp.1050-1058.
[10] Kramer, S.L. and Mayfield, R.T., 2007. "Return period of soil liquefaction". *Journal of Geotechnical and Geoenvironmental Engineering*, 133(7), pp.802-813.
[11] Franke, K.W. and Wright, A.D., 2013. "An alternative performance-based liquefaction initiation procedure for the standard penetration test". *In Geo-Congress 2013: Stability and Performance of Slopes and Embankments III* (pp. 846-849).
[12] Kramer, S.L. and Mayfield, R.T., 2005. "Performance-based liquefaction hazard evaluation". In *Earthquake Engineering and Soil Dynamics* (pp. 1-18).
[13] Cetin, K.O., Seed, R.B., Der Kiureghian, A., Tokimatsu, K., Harder Jr, L.F., Kayen, R.E. and Moss, R.E., 2004. "Standard penetration test-based probabilistic and deterministic assessment of seismic soil liquefaction potential". *Journal of Geotechnical and Geoenvironmental Engineering*, 130(12), pp.1314-1340.
[14] Boulanger, R.W., Wilson, D.W. and Idriss, I.M., 2012. "Examination and reevalaution of SPT-based liquefaction triggering case histories". *Journal of Geotechnical and Geoenvironmental Engineering*, 138(8), pp.898-909.
[15] Cramer, C.H., Rix, G.J. and Tucker, K., 2008. "Probabilistic liquefaction hazard maps for Memphis, Tennessee". *Seismological Research Letters*, 79(3), pp.416-423.
[16] Goda, K., Atkinson, G.M., Hunter, J.A., Crow, H. and Motazedian, D., 2011. "Probabilistic liquefaction hazard analysis for four Canadian cities". *Bulletin of the Seismological Society of America*, 101(1), pp.190-201.
[17] Green, R.A., Bommer, J.J., Stafford, P.J., Maurer, B.W., Kruiver, P.P., Edwards, B., Rodriguez-Marek, A., de Lange, G., Oates, S.J., Storck, T. and Omidi, P., 2020. "Liquefaction hazard in the Groningen region of the Netherlands due to induced seismicity". *Journal of Geotechnical and Geoenvironmental Engineering*, 146(8), p.04020068.
[18] Geyin, M. and Maurer, B.W., 2020. "Fragility functions for liquefaction-induced ground failure". *Journal of Geotechnical and Geoenvironmental Engineering*, 146(12), p.04020142.
[19] Boulanger, R.W. and Idriss, I.M., 2014. *CPT and SPT based liquefaction triggering procedures*. Report No. UCD/CGM.-14, 1.
[20] Molnar, S., Bilson Darko, A., Ghofrani, H., Adhikari, S. and Salsabili, M. 2023. "The Metro Vancouver seismic microzonation mapping project: Overview and multi-method approach to regional geodatabase development". *CCEE-PCEE*, Vancouver, BC, Canada, June 25-30 2023, Paper 258, 8 p.
[21] Molnar, S., 2011. *Predicting earthquake ground shaking due to 1D soil layering and 3D basin structure in SW British Columbia, Canada* (Doctoral dissertation, University of Victoria).
[22] Armstrong, J.E. and Clague, J.J., 1977. "Two major Wisconsin lithostratigraphic units in southwest British Columbia". *Canadian Journal of Earth Sciences*, 14(7), pp.1471-1480.
[23] Clague, J.J., 1976. *Pleistocene sediments in the Northern Strait of Georgia, British Columbia.*
[24] Clague, J.J., Armstrong, J.E. and Mathews, W.H., 1980. "Advance of the late Wisconsin Cordilleran Ice Sheet in southern British Columbia since 22,000 yr BP". *Quaternary Research*, 13(3), pp.322-326.
[25] Clague, J.J., Luternauer, J.L. and Hebda, R.J., 1983. "Sedimentary environments and postglacial history of the Fraser Delta and lower Fraser Valley, British Columbia". *Canadian Journal of Earth Sciences*, 20(8), pp.1314-1326.
[26] Molnar, S., DenToom, A., Assaf, J., Sirohey, A., Boucher, C., Gomez Jaramillo, N., Fyfe, M., and Bilson Darko, A. 2023. Metro Vancouver seismic microzonation mapping: Advancements and guidelines. *CCEE-PCEE*, Vancouver, BC, Canada, June 25-30 2023, Paper 288, 9 p
[27] Robertson P.K. and Cabal K.L. 2015. *Guide to cone penetration testing for geotechnical engineering*, Gregg drilling. 6th edition.
[28] Youd, T.L., Idriss I.M., Andrus, R.D., Arango, I., Castro, G., Christian, J.T., et al. 2001. " Liquefaction resistance of soils: summary report from the 1996 NCEER and 1998 NCEER/NSF workshops on Evaluation of Liquefaction Resistance of Soils". *Journal of Geotechnical and Geoenvironmental Engineering*, 127 (10): 817–33.
[29] Boulanger, R.W. 2003. "High Overburden Stress Effects in Liquefaction Analyses". *Journal of Geotechnical and Geoenvironmental Engineering*, ASCE 129 (12): 1071–082.

[30] Idriss, I.M. 1999. *An Update to the Seed-Idriss simplified procedure for evaluating Liquefaction potential, In Proceedings, TRB Workshop on new approaches to liquefaction.* Publication No. FHWARD-99-165, Federal Highway Administration, January.
[31] Andrus, R.D., Stokoe, K.H. and Hsein Juang, C., 2004. "Guide for shear-wave-based liquefaction potential evaluation". *Earthquake Spectra*, 20(2), pp.285-308.
[32] Robertson, P.K., Woeller, D.J. and Finn, W.D.L., 1992. "Seismic cone penetration test for evaluating liquefaction potential under cyclic loading". *Canadian Geotechnical Journal*, 29(4), pp.686-695.
[33] Youd, T. L., Harp, E. L., Keefer, D. K., and Wilson, R. C., 1985. "The Borah Peak, Idaho earthquake of October 28, 1983, chap. on Liquefaction". *Earthquake Spectra*, 2 (4): 71–89.